Energy 157 (2018) 448–459

Contents lists available at ScienceDirect

Energy

journal homepage: www.elsevier.com/locate/energy

Thermal performance of solid walls in a mesoscale combustor with a plate flame holder and preheating channels

Jianlong Wan, Haibo Zhao*

State Key Laboratory of Coal Combustion, School of Energy and Power Engineering, Huazhong University of Science and Technology, Wuhan 430074, China

ARTICLE INFO

Article history:
Received 21 January 2018
Received in revised form
17 April 2018
Accepted 28 May 2018
Available online 29 May 2018

Keywords:
Plate flame holder
Preheating channel
Preheating effect
Heat-loss effect
Flame height

ABSTRACT

The flame is very hard to keep steadily symmetrical for a wide flammability limit under some extreme combustion conditions (such as large heat loss and fuel of low caloric value). Recently, we manufacture a mesoscale combustor with a plate flame holder and preheating channels, which could take the advantage of the flow recirculation and heat recirculation effects. The experimental results show that this special configuration performs excellent in flame-anchoring, and the flame can remain steadily symmetrical at very low equivalence ratio in the normal environment. In order to provide theoretical basis to optimize this combustor, the three-dimensional numerical simulation is used to study the thermal performances of solid walls on unburned fuel mixture quantitatively. The results indicate that the combustor wall does not always have preheating effects on the unburned mixture. Some walls or some parts of walls have the negative effect of heat loss. Furthermore, some interesting boundary shapes of the preheating areas or heat loss areas are found. It is deduced that the thermal performances of combustor walls mainly depend on the side with higher temperature. In addition, the preheating area decreases with an increasing flame height, so a lower flame height is probably beneficial for preheating.

1. Introduction

Under some extreme combustion conditions, such as large heat loss due to a big surface-area-to-volume ratio or heat-transfer coefficient, the short residence time of gaseous mixture and the fuel mixture of low concentration/caloric-value, the flames in the combustors easily lose stability. As a result, various unstable flame behaviors appear [1,2], such as the flame with repetitive extinction and ignition [3–5], asymmetric and oscillating flames [6,7] and the spinning flame [8,9]. These unstable flame propagation modes are bad for the safety and efficient operation of combustors which serve as the heat resource for the mesoscale thermophotovoltaic or power systems.

In order to solve the issues above, many methods have been employed to improve the flame stabilization. For instance, some researchers used the burned exhaust gas of high temperature to preheat the incoming unburned mixture via some special structures and solid material, which can not only improve the inlet temperature of fuel mixture but also decrease the heat-loss rate. These combustors with special structures include the “Swiss-roll” burner [10–12], a low-heat-loss combustor with porous media wall [13], the combustor inserted by porous media [14,15] and so on. Their results indicated that the flammability limits could be significantly extended via these heat management ways. In addition, Veeraragavan [16,17] pointed out that the wall made of a special material (orthotropic thermal conductivity material) could create “hot pockets” in the wall which could stabilize the flame propagation in a parallel plate burner.

However, the flame could not be effectively anchored in combustors above, which led to the relatively narrow flame blow-off limits. Therefore, some researchers adopted the flow recirculation effect to solve this shortcoming. For instance, many structures had eminent performances in anchoring flame based on the flow recirculation effect, such as bluff body [18,19], wall cavity [20] and backward facing step [21–26]. The results showed that these structures which generated flow recirculation could significantly extend the flame blow-off limits, but the flammable range of fuel mixture in these combustors is small. Therefore, it is expected that the flame stabilization including both the flammability limit and blow-off limit can be both improved if the heat recirculation and flow recirculation are efficiently combined. Actually, some researchers recently developed some combustors with special

* Corresponding author. State Key Laboratory of Coal Combustion, Huazhong University of Science and Technology, 1037 Luoyu Road, Wuhan 430074, China.
E-mail addresses: klinsmannzhb@163.com, hzhao@hust.edu.cn (H. Zhao).

https://doi.org/10.1016/j.energy.2018.05.189
0360-5442/

structures mentioned above to improve the flame stabilization. For example, Yadav et al. [27] and Fan et al. [28] manufactured the three step micro-combustor with a heating cup and the mesoscale Swiss-roll combustor with a bluff body, respectively. Their results showed that this strategy could not only effectively anchor the flame but also remarkably extend the flammability limits.

Nevertheless, the mechanisms of the synergistic effect of heat recirculation and flow recirculation on improving the flame stability and influencing the flame dynamics are not systematically studied so far. For this purpose, we developed a micro combustor with a plate flame holder and preheating channels, which could jointly utilize the heat recirculation and flow recirculation effects. The incoming unburned fuel mixture can be well preheated in the preheating channels, and then the flow recirculation (recirculation zone and low velocity zone) behind the flame holder can well anchor the flame front. In turn, the flame anchored by the flame holder can better preheat the fresh fuel mixture, which results in a more obvious thermal expansion effect and then contributes to a faster flow velocity. As a result, the recirculation zone is enlarged. These favorable factors can significantly improve the flame stabilization. Our previous two-dimensional numerical results showed that lean CH_4/air premixed flames could be stabilized in the micro combustor with a plate flame holder and preheating channels within a large range of inlet velocity and revealed the dynamic process of flame blow-off in the meanwhile [29,30]. Furthermore, the preliminary result in Ref. [29] indicated that the flame holder and combustor wall sometimes have the negative effect of heat loss on the incoming unburned mixture. The thermal performance can significantly affect the flame structure and dynamic characteristics [1,8,16], but the relevant issues are not systematically studied.

Therefore, the present paper quantitatively investigates the thermal performance of solid wall in the combustor with a plate flame holder and preheating channels. Understanding the thermal performance of combustor wall can give hints to optimize the present combustor. The present work is the first step of our systematical work which studies the synergistic effect of heat recirculation and flow recirculation on flame dynamics. In the future, the flame topology structure, the flame anchoring and blow-off mechanisms, the flame behaviors and the transition characteristics of flame behaviors under the above synergistic effect will be investigated experimentally and numerically in detail. In addition, the combustion characteristics of different fuels in the present combustor are also necessary to reveal, which can provide theoretical basis to choose the appropriate fuels.

2. Experimental

2.1. Experimental setup and methods

Fig. 1 shows the experimental system in present work. Methane and air are fully mixed in a mixing tank before entering the combustor. The equivalence ratio (ϕ) and inlet velocity (V_{in}) of CH_4/air premixed mixture are controlled by two mass-flow meters. For the sake of safety, a flash-arrester is installed in the fuel mixture line. A digital video camera (Canon EOS 6D with the recording frequency of 25 Hz) is applied to take photographs. The unburned mixture is ignited by a flame gun at the combustor exit. A temperature measurement system via dynamic transient method developed by Xu et al. [31,32] is placed at the center of combustor exit to measure the temperature of the exhaust gas. In addition, the present work mainly focuses on the laminar flame under lean fuel because the greatest advantage of the present combustor is to keep stable flame and achieve high efficient combustion under some extreme combustion conditions as mentioned above.

The combustor is manufactured by the transparent quartz glass,

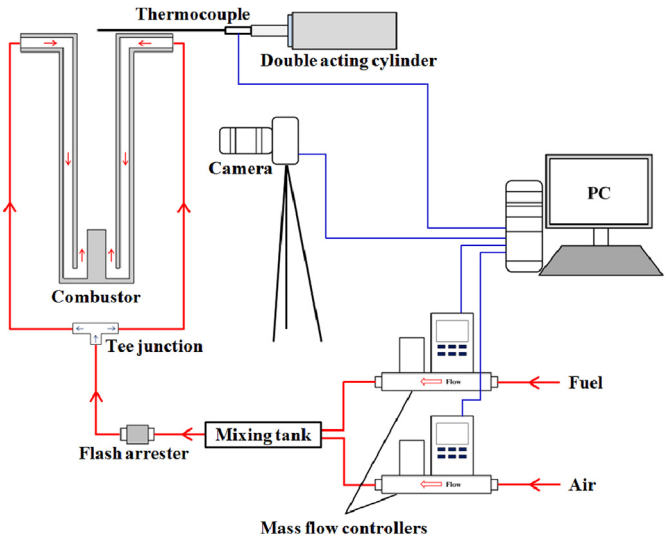

Fig. 1. Schematic diagram of the experimental system.

which is vertically placed, as shown in Fig. 2. For clarity, the whole channel of the combustor is divided into two segments by two blue dashed lines along with the upper wall of the flame holder, *i.e.*, the preheating channels and the combustion chamber. Additionally, the solid wall of the combustor is divided into four segments by the

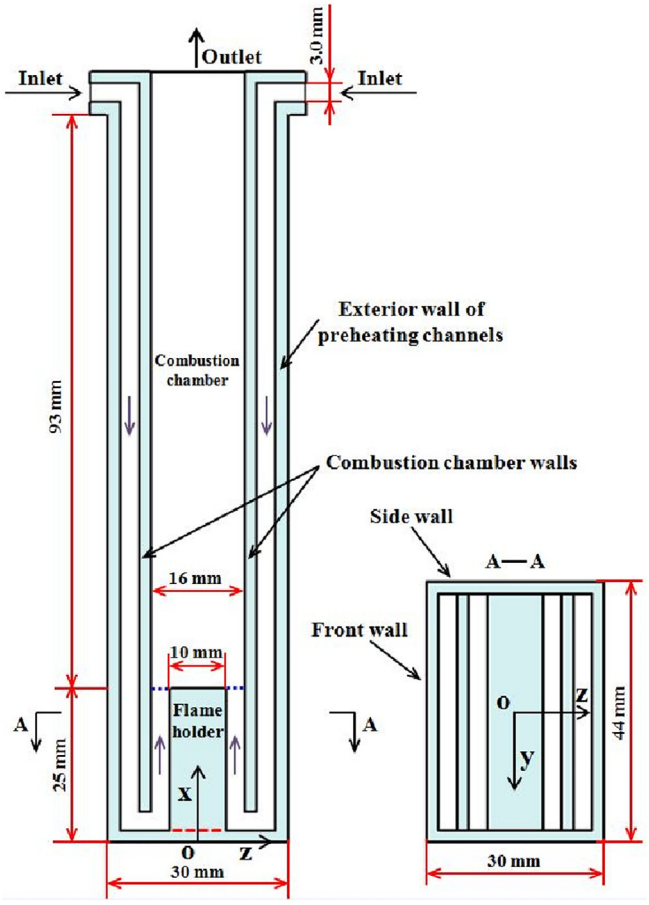

Fig. 2. Cross-section schematic of the mesoscale combustor with a plate flame holder and preheating channels.

red dashed lines: the plate flame holder, the integrated exterior wall of two preheating channels, and two combustion chamber walls. The wall thickness (δ) is 2.0 mm, and the gap and width of the preheating channel are 3.0 mm and 40.0 mm, respectively. The gap of the combustion chamber is 16.0 mm. Besides, the width, length and height of the flame holder are 40.0 mm, 10.0 mm and 23.0 mm (25.0 mm-2.0 mm), respectively. Other geometrical dimensions are shown in Fig. 2.

Fig. 3a shows that the combustor is symmetrical with respect to the horizontal and vertical center parting planes, which also clearly demonstrates the locations of the front, bottom and side walls. Considering the finite computational resources and accuracy requirements for numerical simulation, one of the four equal parts of the combustor is adopted as the computational region as the right-lower shaded region in Fig. 3b. The two parting planes (blue surfaces) in Fig. 3c are set as the symmetry boundaries. It can be seen from Fig. 2a and c that the side view shows the *x*-*z* plane, and the front view shows the *x*-*y* plane.

At the beginning of the experiment, the fresh fuel mixture is ignited firstly at the exit of combustor for $\phi = 0.6$ at which the flame can be stabilized near the flame holder, and then we decrease the equivalence ratio with a step of 0.025 under a constant inlet velocity until flame blows off. As an example, $V_{in} = 1.0$ m/s is adopted in this paper (the corresponding Reynolds number based on the preheating channel gap is 200).

2.2. Experimental results

Fig. 4 presents the side views of stable flame at different equivalence ratios, which shows that the flame still can remain symmetrically stable in the combustion chamber under a very small equivalence ratio (such as $\phi = 0.45$), which indicates that the present combustor can remarkably broaden the flammability limit. In addition, as the decrease in the equivalence ratio, the flame becomes more and more slender, and the distance between the right and left flame fronts obviously decreases so that the right and left flame roots at $\phi = 0.45$ merge into one "U-shape" flame root, and the distance between the right and left flame fronts near the middle position of flame front is narrower than the width of flame root (see the white arrow in Fig. 4d). When the equivalence ratio decreases to 0.425 further, the flame pinch-off phenomenon will occur, and the flame blows off in the end. It should be pointed out that as the images of stable flames in Fig. 4 were taken from the side, the horizontally (*y*-direction) superimposed effect of the flame front made the flame appear thicker. In a word, the present special structure can significantly improve the flame stabilization.

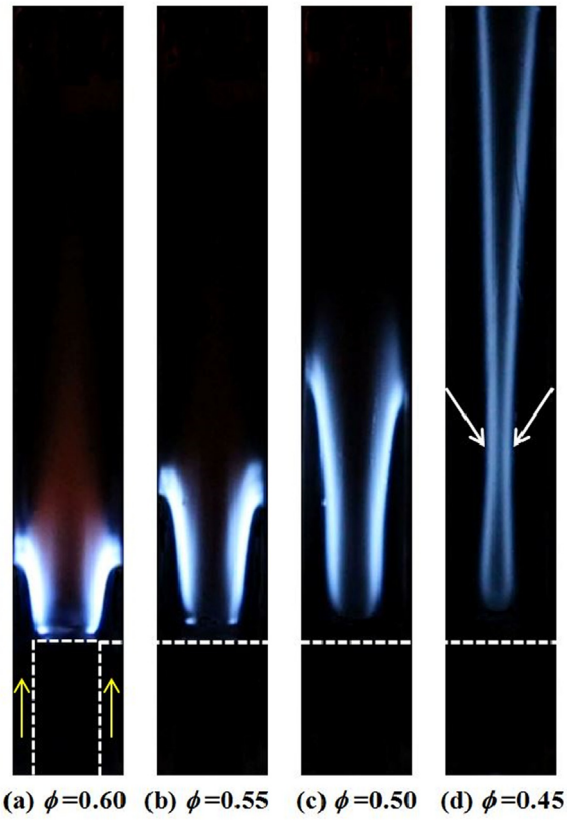

Fig. 4. Side view photographs of stable flame under different equivalence ratios at $V_{in} = 1.0$ m/s (the end wall of flame holder is marked by the horizontally dashed lines, the yellow arrow indicates the flow direction of fresh mixture). (For interpretation of the references to colour in this figure legend, the reader is referred to the Web version of this article.)

3. Numerical analysis

3.1. Computation scheme

The thermal conductivity of quartz glass is 2.0 W/(m·K) [8]. The CFD software Fluent 14.0 is applied to solve the momentum, mass, energy and species conservation equations [33]. The detailed C1 chemistry mechanism including 18 species and 58 elementary reactions is adopted to simulate CH_4/air premixed combustion [34]. The thermodynamic and transport properties of the gaseous species are taken from the CHEMKIN databases [35,36]. As the heat conduction in the solid walls can significantly affect the flame

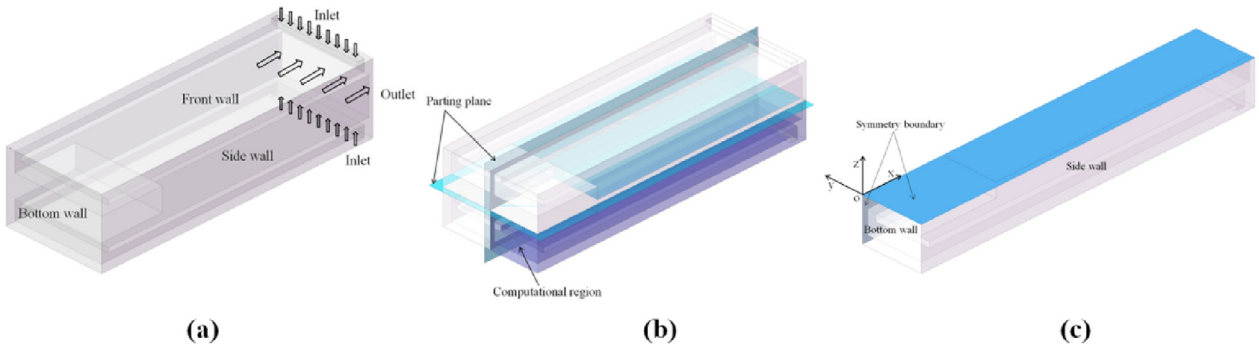

Fig. 3. Three-dimension schematic of the mesoscale combustor with a plate flame holder and preheating channels.

propagation characteristics [16], the heat fluxes in the solid wall are taken into computation using the Fourier's law. The inner surfaces of combustor are assumed to be chemically inert and no-slip. The CH_4/air premixed mixture of 300 K with uniform concentration and velocity distribution is set at the combustor inlet. A Neumann boundary condition is given for the combustor exit. The heat loss rate from the combustor outer wall is calculated by $q = h_s(T_{W,O} - T_\infty) + \varepsilon_s\sigma_s(T_{W,O}^4 - T_\infty^4)$, Where $T_{w,o}$ is the temperature of outer surface, T_∞ is the ambient temperature (300 K), h_s is the heat transfer coefficient of natural convection (5.0 W m^{-2} K^{-1}) [37], ε_s is the surface emissivity (0.92) [38], and σ_s is the Stephan-Boltzmann constant (5.67×10^{-8} W m^{-2} K^{-4}).

In addition, grid independency is checked by using three sets of grid system ($\Delta x = \Delta y = \Delta z = 250$ μm, 200 μm and 125 μm). It is found that the cell size of 250 μm is sufficiently fine to capture the flame structure (see Fig. S1 in supplementary materials) via comparing the HCO and CH (two key radicals) distributive profiles near the flame front. Further refinement on the meshes near the flame holder is conducted, and a non-uniform grid system with 1,562,592 cells is employed in final computation.

3.2. Model validation

To evaluate the accuracy of the present numerical model, our previous work compared the lean flammability limits under different inlet velocities via experiment and simulation, and results showed that the predicted and measured lean flammability limits were almost same (see Fig. S2a in supplementary materials). The maximum relative deviation between them is 5.88% at $V_{in} = 1.0$ m/s. Moreover, the temperatures of the predicted and measured exhaust gas at different equivalence ratios and inlet velocities were compared, and results demonstrated that predicted results agreed reasonably with experimental data. The maximum relative error is 9.87% at $V_{in} = 0.8$ m/s and $\phi = 0.6$, while the minimum one is only 3.20% at $V_{in} = 0.6$ m/s and $\phi = 0.6$ (see Fig. S2b in supplementary materials). In addition, the flame shapes and geometrical sizes via experimental measurement and numerical simulation were also compared, as shown in Figs. 5 and 6. Fig. 5 presents that the shapes of observed and predicted flame are very similar, and Fig. 6 quantitatively indicates that the heights of flame front in experiment and simulation are almost same. The maximum relative error is 9.65% at $\phi = 0.55$, while the minimum one is only 0.51% at $\phi = 0.50$. The error bar in Fig. 6 is the flame height fluctuation mainly caused by the environment perturbation (such as the perturbation of heat loss coefficient). These results confirm the reasonable accuracy of the numerical model adopted in present work.

3.3. Definition of flame front

The Heat-Release Rate (HRR) is always used to identify the flame front [39], which is also adopted in present paper. To elucidate this, we display the net reaction rate contours of methane with overlaid normalized isoline of 10% maximum HRR, which has been normalized by their maximum values, at $\phi = 0.55$ in Fig. 7. It demonstrates that the high-reaction-rate zone of methane lies in the scope of normalized isoline of 10% maximum HRR. Similar structures are also observed in other cases. Therefore, we use the normalized isoline of 10% maximum HRR to mark the flame front.

3.4. Thermal performance of each solid wall

It is well known that the heat recirculation via solid wall has a significant effect on combustion characteristics in combustors [16,17], especially for the combustor with preheating structure.

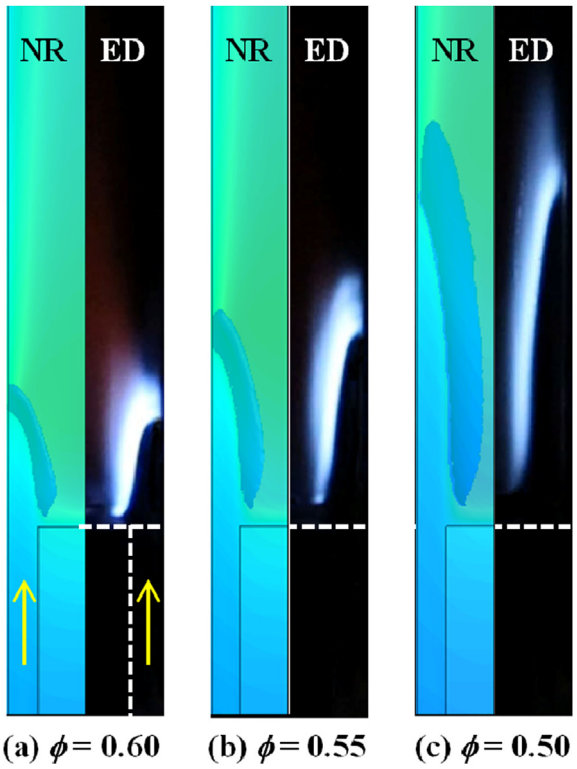

Fig. 5. Flame shapes for different equivalence ratios at $V_{in} = 1.0$ m/s from side-view via experimental measurement and numerical simulation (ED and NR mean the experimental datum and numerical result, respectively).

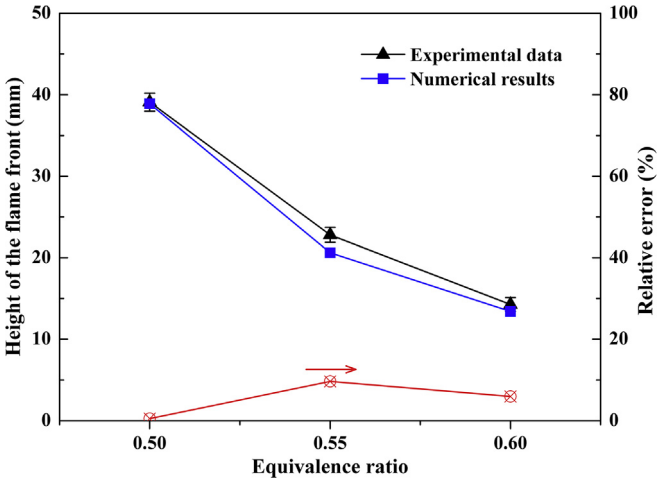

Fig. 6. Flame height for different equivalence ratios at $V_{in} = 1.0$ m/s via experimental measurement and numerical simulation.

However, not every wall or a whole wall always has preheating effect on the unburned mixture. Maybe some walls or some parts of walls act as the negative effect of heat loss for the incoming unburned mixture. In order to give guidance to optimize the present combustor (such as choosing the suitable height of the flame holder), the following sections will quantitatively discuss the thermal performances of solid walls.

3.4.1. Temperature distribution characteristics of the combustor

At first, Fig. 8 displays the temperature fields of the combustor for different *x-y* sections. Fig. 8d and e indicate that there are two

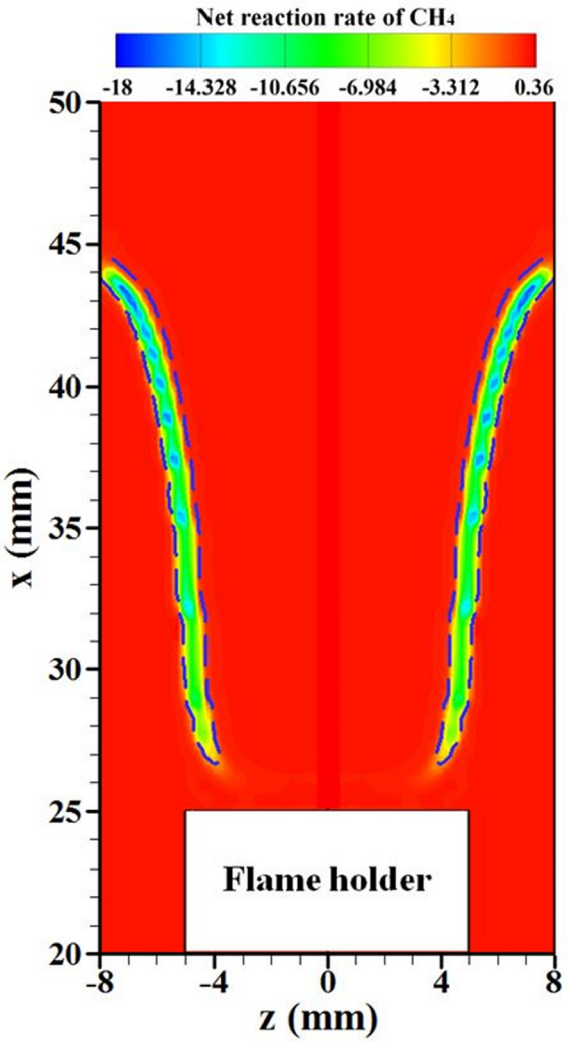

Fig. 7. Net reaction rate contours of CH_4 with overlaid normalized isoline of 10% maximum HRR (blue dashed line) at y = 0.0 mm cross-section and $\phi = 0.55$. (For interpretation of the references to colour in this figure legend, the reader is referred to the Web version of this article.)

high-temperature zones in the combustion chamber wall: one is near the flame front (the upstream one) while another zone is near the combustor exit (the downstream one). This is mainly because that the heat transfer coefficient of unburned mixture near the middle combustion chamber wall (~60 mm ≤ x ≤ 90 mm) in the preheating channel is larger due to a faster flow velocity which results from the thermal expansion effect in a more upstream preheating channel, and this cooling effect leads to a local lower-temperature combustion chamber wall. As a result, the burned mixture temperature in this region (~60 mm ≤ x ≤ 90 mm) is also lower. The inner wall of preheating channel wall is heated by the external surface of combustion chamber wall via the heat radiation, and its temperature level is significantly lower than that of the surface at $z = -10$ mm. Therefore, it can be deduced that the unburned mixture in the preheating channel is mainly preheated by the combustion chamber wall, which will be confirmed in the following sections.

Moreover, we also present the temperature fields with overlaid 10% maximum HRR isoline for different x-z slices. Fig. 9 shows that the temperature level is decreasing when approaching the side wall, and there are also two high temperature zones in the side wall (see Fig. 9g and h), which are caused by the distribution characteristic of gas temperature in the combustion chamber. More importantly, Fig. 9 shows that the unburned mixture is not always preheated by the solid wall. For instance, Fig. 9a presents that the temperature of unburned mixture in a more downstream preheating channel is higher than that of the solid wall (~2.0 mm ≤ x ≤ 30 mm), which means that the solid wall absorbs heat from the unburned mixture. The following sections will quantitatively reveal the thermal performance of every solid wall in detail.

3.4.2. Thermal performance of vertical surface of flame holder

The flame holder can not only generate flow recirculation to anchor the flame but also affect the flame stability via thermal performance on unburned mixture. Fig. 10a shows that the wall temperature of flame holder is higher at a more downstream location, and it is lower near the side wall ($y = -19$ mm) due to the heat loss. Fig. 10b displays the temperature difference very near the inner wall between the inner wall and gaseous mixture, and the positive values mean that the unburned mixture is preheated by the inner wall, while negative values mean the opposite (*i.e.*, the inner wall absorbs heat from unburned mixture). It can be seen that most part of flame holder can preheat the unburned mixture. Based on Fig. 10b, we draw the thermal performance of inner wall at $z = -5$ mm and 5 mm on unburned mixture in Fig. 10c. On the one hand, Fig. 10c demonstrates that the upper preheating area slightly decreases when approaching the side wall firstly (~−15 mm ≤ y ≤ 15 mm), which consists with the shape of the vertical wall temperature isoline of plane flame holder near $x = 10.0$ mm (see Fig. 8b). Then, the preheating area increases sharply very near the side wall (~19 mm ≤ y ≤ 20 mm and ~-20 mm ≤ y ≤ −19 mm) due to the relative high-temperature side wall of the combustion chamber. As a result, the boundary between the upper preheating area and heat loss area presents the “M” shape. On the other hand, Fig. 10c indicates that the lower preheating area also decreases firstly (~−19 mm ≤ y ≤ 19 mm) and then increases very near the side wall (~19 mm ≤ y ≤ 20 mm and ~-20 mm ≤ y ≤ −19 mm) when approaching the side wall, which consists with the shape of the temperature isoline of unburned mixture in the preheating channel at x = ~3.0 mm (see Fig. 8c). As a result, the boundary between the lower preheating area and heat loss area appears the “W” shape. Overall, the unburned mixture near the flame holder is preheated to a higher level before entering the combustion chamber (see Fig. 10a).

3.4.3. Thermal performance of inner surface of combustion chamber wall

Fig. 9 has indicated that the inner surface of combustion chamber wall is in the two channels (*i.e.*, the preheating channel and combustion chamber, as shown in Fig. 11a), so the inner walls at $z = -8$ mm and 8 mm might have three kinds of thermal performance, *i.e.*, absorbing heat from the high-temperature burned mixture behind the flame front in the combustion chamber, preheating effect on the unburned mixture and absorbing heat from the unburned mixture in front of the flame front. It can be seen from Fig. 11a that every temperature profile has two peaks, which results from the temperature distribution characteristics of burned mixture in the combustion chamber. The inner wall temperature reaches the highest value near the flame front at ~ $x = 50$ mm, and it is decreasing sharply along the transverse (y) direction (from $y = 0$ mm to $y = -20$ mm). The negative temperature difference between the inner wall and gas mixture in the downstream chamber behind the flame front (~x > 15 mm) indicates that the walls absorb heat from the high-temperature burned mixture, while the negative values in the upstream chamber in front of the

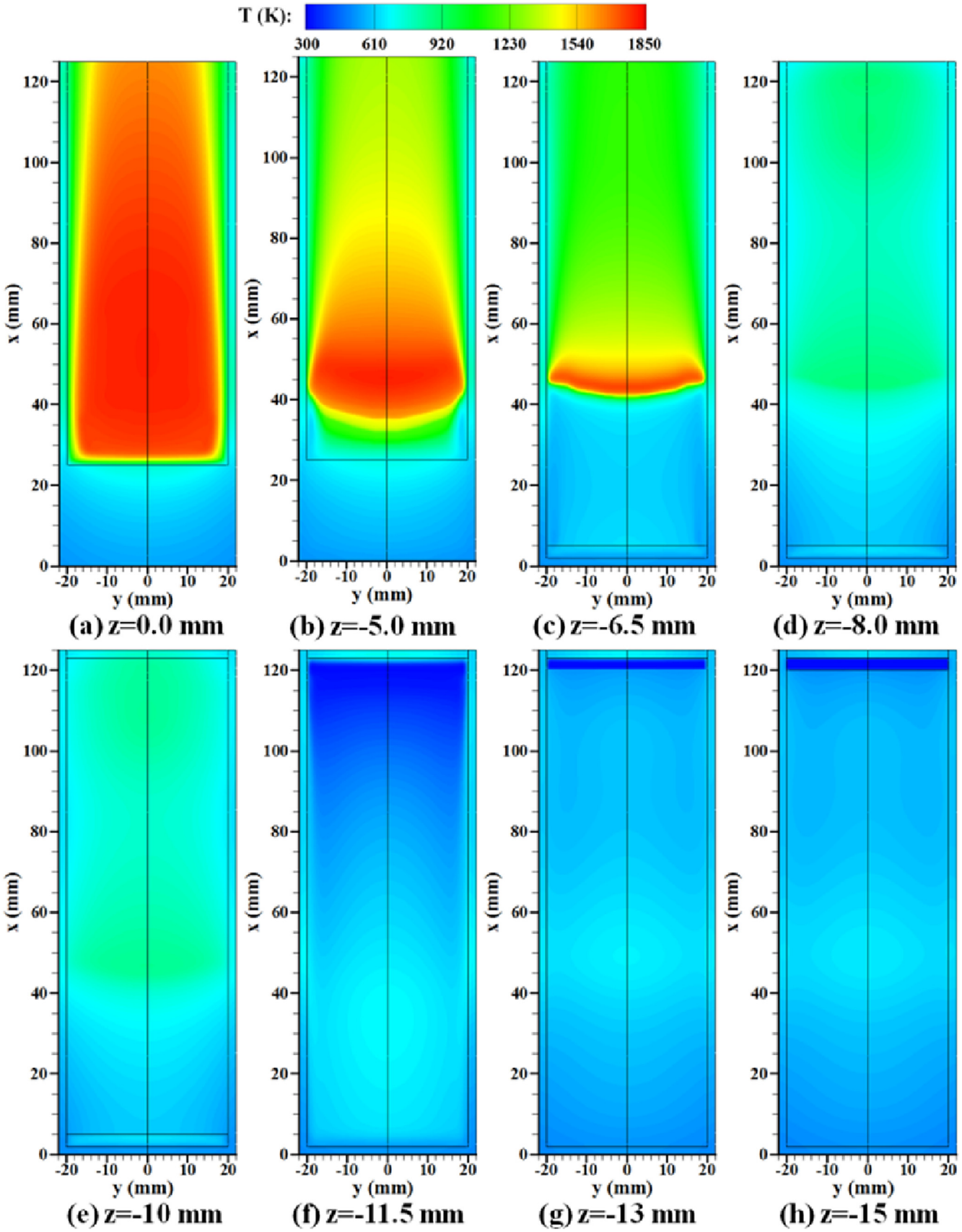

Fig. 8. Temperature fields of the combustor for different *x*-*y* sections at $\phi = 0.55$.

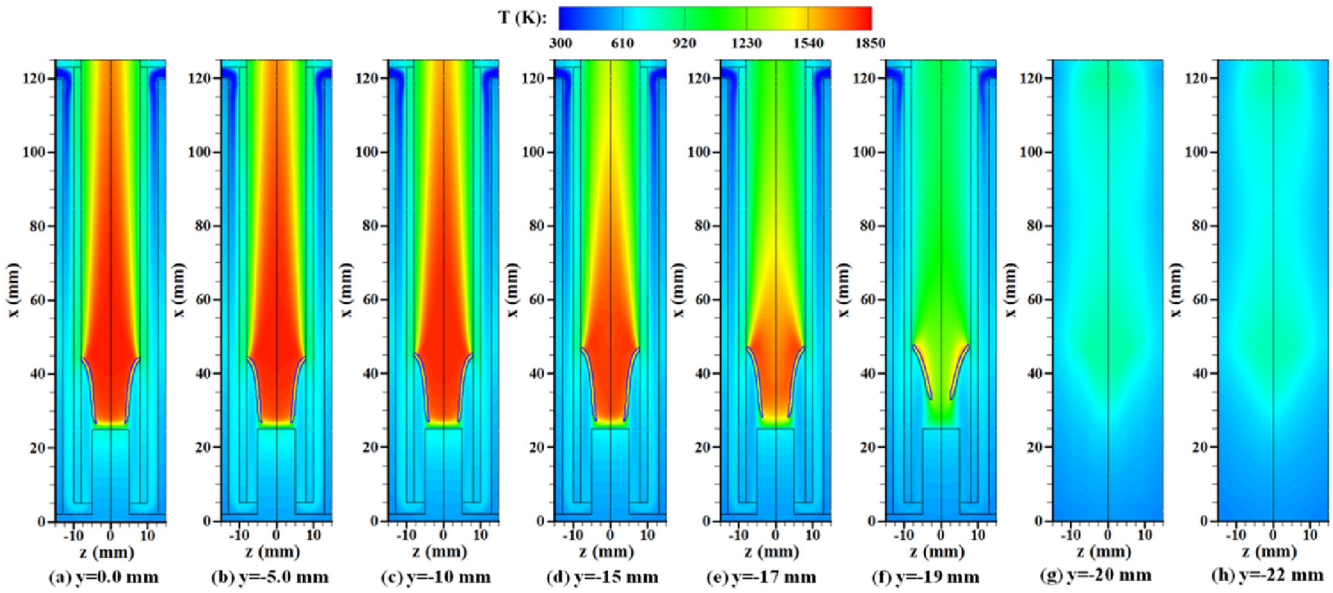

Fig. 9. Temperature contours with overlaid 10% maximum HRR isoline (blue solid lines) for different *x-z* sections at $\phi = 0.55$. (For interpretation of the references to colour in this figure legend, the reader is referred to the Web version of this article.)

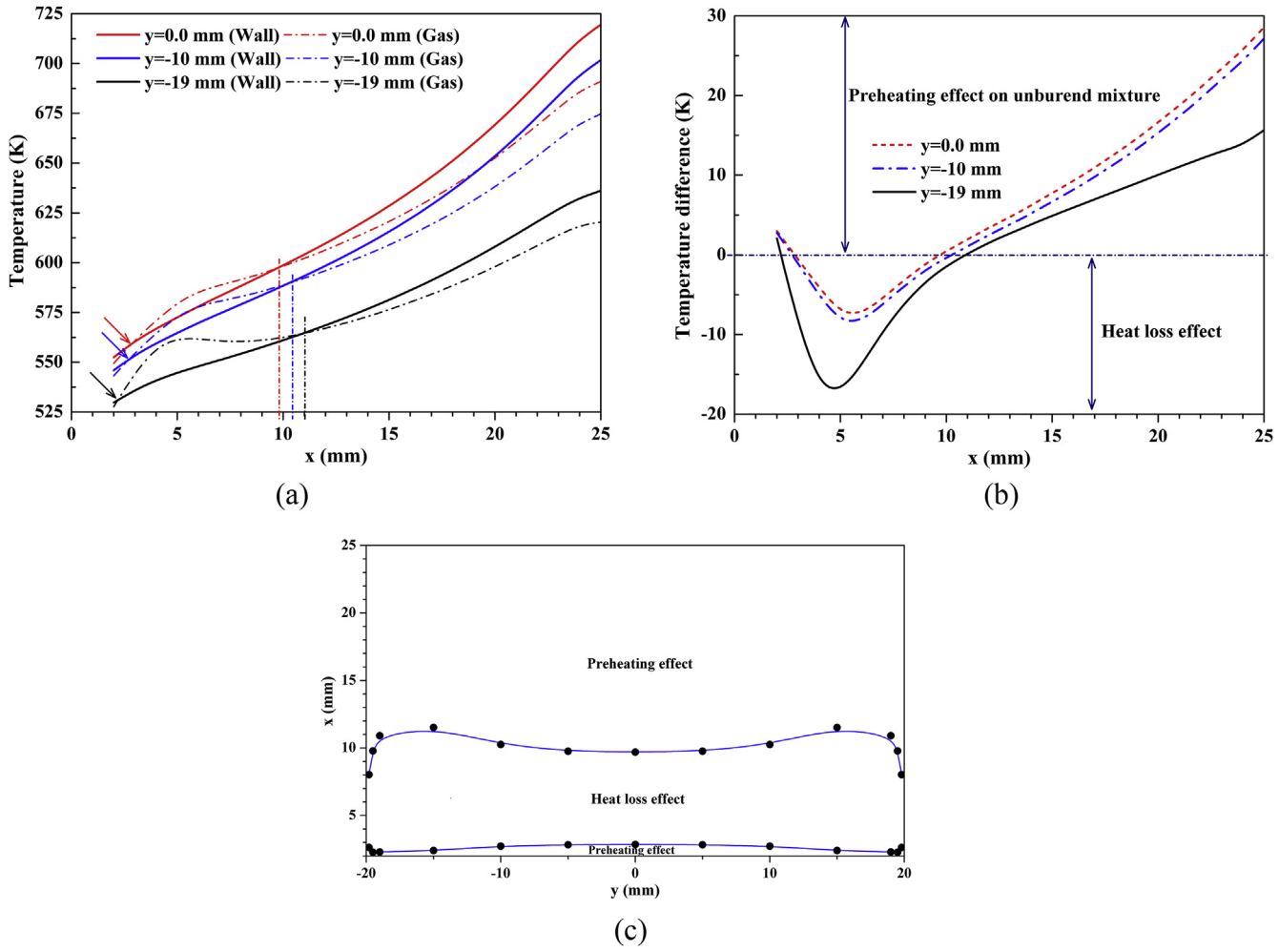

Fig. 10. Vertical wall temperature profiles of plane flame holder (z = −5 mm and 5 mm) and the gas temperature profiles very near the inner wall (z = −5.2 mm and 5.2 mm) (a) and the temperature difference between them (b) for three *x-z* sections at $\phi = 0.55$, and the thermal performance distributions of wall on unburned mixture (c).

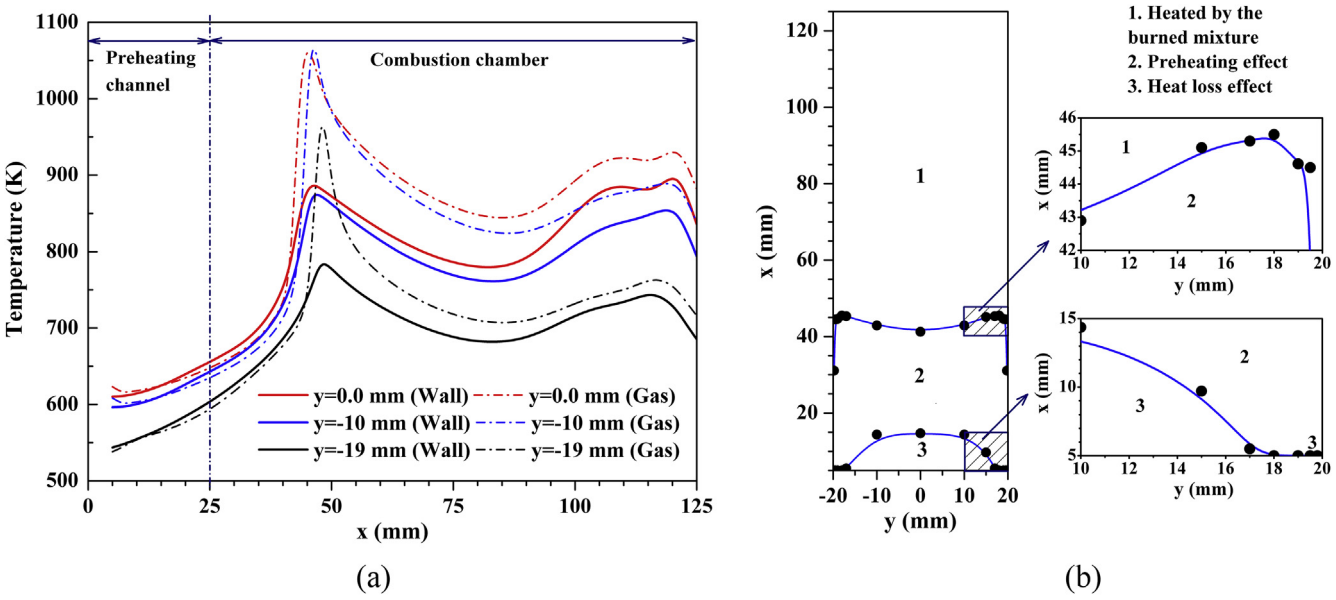

Fig. 11. Inner surface ($z = -8$ mm and 8 mm) temperature profiles of combustion chamber wall and the gas temperature profiles very near the inner wall ($z = -7.8$ mm and 7.8 mm) for three x-z sections at $\phi = 0.55$ (a) and the thermal performance of inner wall (b).

flame front (~x < 15 mm) indicate that the walls absorb heat from the incoming unburned mixture. Based on these results, we draw the thermal performance distributions of inner wall at $z = -8$ mm and 8 mm in Fig. 11b. Fig. 11b shows that most inner wall are heated by the high-temperature burned mixture in the combustion chamber, and the preheating area presents a constricted "waist" shape (-18 mm $\leq y \leq 18$ mm). However, the preheating area decreases sharply very near the side wall (~18 mm $\leq y \leq 20$ mm and ~-20 mm $\leq y \leq -18$ mm). As a result, the upper boundary of preheating area presents the "M" shape, and the lower boundary of preheating area presents the arch shape. These change rules consist with the temperature distribution characteristic of gaseous mixture near the combustion chamber wall (see Fig. 8c). Therefore, it is deduced that the thermal performance distribution characteristic of inner wall of combustion chamber wall mainly depends on the temperature distribution characteristic of gaseous mixture near combustion chamber wall.

3.4.4. Thermal performance of external surface of combustion chamber wall

Moreover, Fig. 12a shows the external surface temperature ($z = -10.0$ mm) of combustion chamber wall, which indicates that the unburned mixture is mainly preheated in the upstream preheating channel (~45 mm $\leq x \leq$ 120 mm), and its temperature reaches the highest level near the middle preheating channel (~$x = 50$ mm). It is interesting to find that there are troughs in the gas temperature profiles in the more upstream channel (~$x = 120$ mm). This is mainly because that the unburned mixture

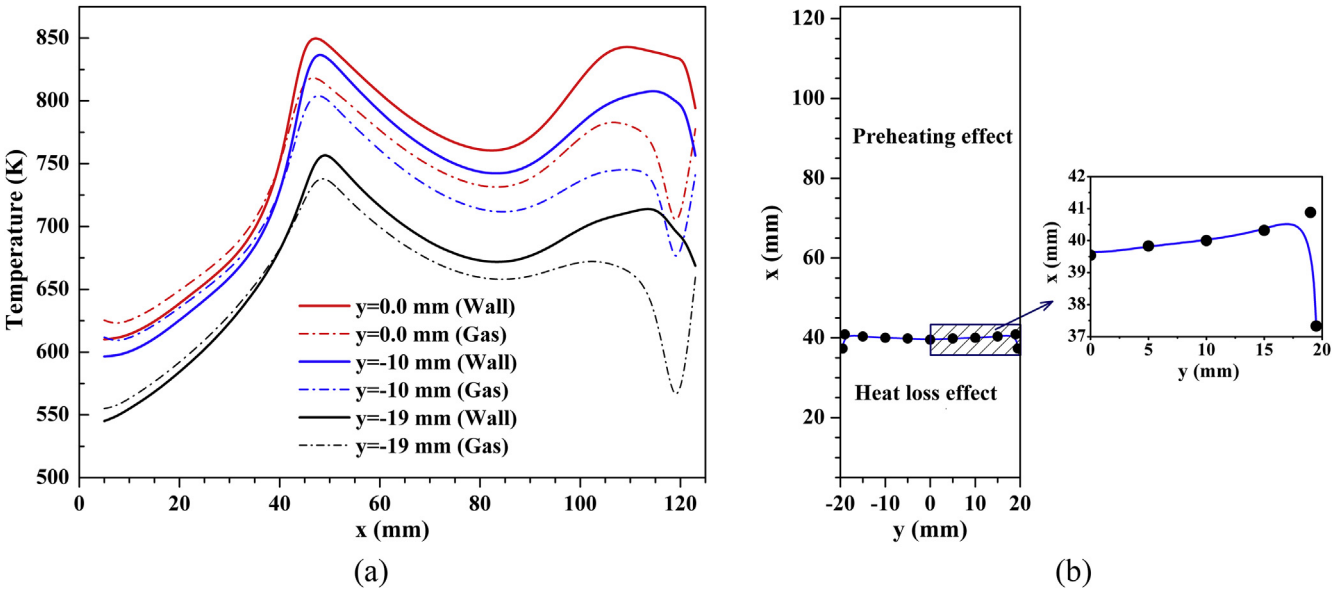

Fig. 12. External surface ($z = -10$ mm and 10 mm) temperature profiles of combustion chamber wall and the gas temperature profiles very near the inner wall ($z = -10.2$ mm and 10.2 mm) for three x-z sections at $\phi = 0.55$ (a) and the thermal performance distributions of wall on unburned mixture (b).

in the flow recirculation zone at ~120 mm ≤ x ≤ 123 mm can be preheated to a higher temperature due to the longer residence time. Fig. 12b shows the thermal performance of inner wall at $z = -10$ mm, which indicates that the preheating area is slightly decreasing when approaching the side wall at first, which consists with the temperature isoline shape of external surface of combustion chamber wall near $x = 40.0$ mm (see Fig. 8e). Then, the preheating area increases sharply very near the side wall (~19 mm ≤ y ≤ 20 mm and ~−20 mm ≤ y ≤ −19 mm) owing to the heat transferred from the side wall of combustion chamber. As a result, the boundary between the preheating area and heat loss area appears the "M" shape. This demonstrates that the distribution characteristic of thermal performance on the incoming unburned mixture is mainly determined by the external surface of combustion chamber wall.

3.4.5. Thermal performances of inner surface of preheating channel wall

Besides, the inner surface of preheating channel wall (z = −13 mm) also has heat effects (preheating effect or heat loss effect) on unburned mixture although its temperature level is low. Fig. 13a indicates that the unburned mixture is mainly preheated in the upstream preheating channel (~50 mm ≤ x ≤ 120 mm), so the temperature of the unburned mixture can reach the highest level near the middle channel (~x = 50 mm). It should be pointed out that there are not two peaks of temperature profile in Fig. 13a, which means that the influence of temperature distribution characteristics (two high temperature zones) of burned mixture near the combustion chamber wall on the inner wall of preheating channel wall is relatively small. The mixture temperature in the downstream channel (~x ≤ 50 mm) is decreasing when approaching the side wall, but the gas temperature in the more upstream channel (~110 mm ≤ x ≤ 120 mm) near the side wall ($y = -19$ mm) is higher caused by the high-temperature side wall of preheating channel (see Fig. 9g and h). Fig. 13b, which shows the thermal performance of inner wall at $z = -13$ mm, indicates that the heat loss area decreases firstly and then increases sharply very near the side wall (~15 mm ≤ y ≤ 20 mm and ~−20 mm ≤ y ≤ −15 mm) when approaching the side wall, which consists with the shape of the temperature isoline of unburned mixture at x = ~40.0 mm in the preheating channel (see Fig. 8f). As a result, the "W" shape boundary between the preheating area and heat loss effect area occurs. Based on these results, we deduce that the thermal performance of the inner surface of preheating channel wall mainly depends on the distribution characteristic of the unburned mixture temperature in the preheating channel.

In addition, as the surface areas of the side and bottom walls are much smaller than that of the combustion chamber wall and preheating channel wall, it is expected that their heat effects on the incoming unburned mixture is negligible. Therefore, we just discuss the thermal performances of the combustion chamber wall and preheating channel wall on unburned fresh mixture in present paper.

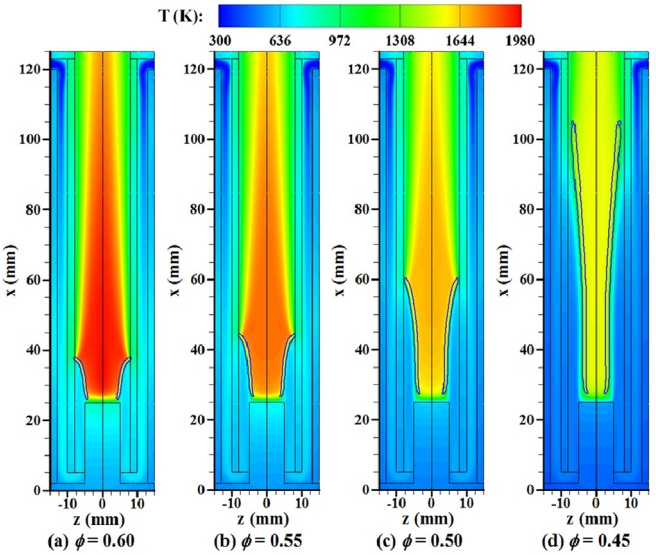

Fig. 14. Temperature contours with overlaid 10% maximum HRR isoline (blue solid lines) at y = 0.0 mm section for different equivalence ratio. (For interpretation of the references to colour in this figure legend, the reader is referred to the Web version of this article.)

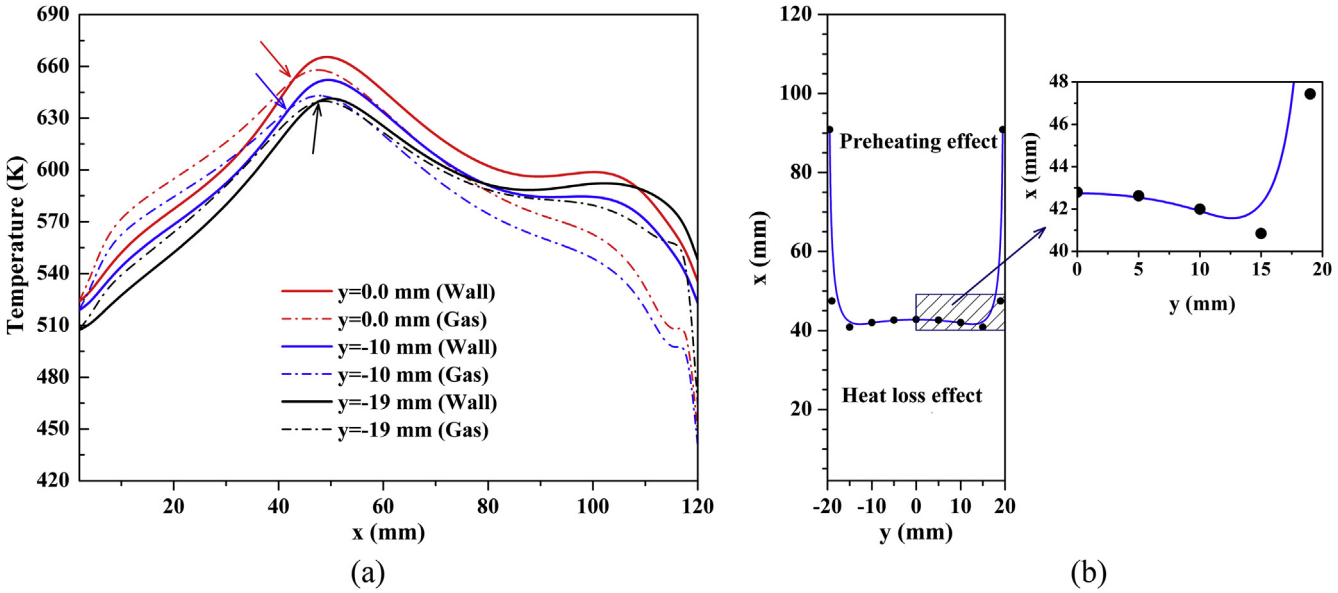

Fig. 13. Inner surface temperature profiles of preheating channel wall ($z = -13$ mm) and the gas temperature profiles very near the inner wall ($z = -12.8$ mm) for three x-z sections at $\phi = 0.55$ (a) and the thermal performance distributions of wall on unburned mixture (b).

3.5. Effect of equivalence ratio

3.5.1. Effect of equivalence ratio on temperature distribution

It can be expected that the height of flame front which is affected by the equivalence ratio in the combustion chamber can significantly affect the thermal performance of solid walls. Taking this into consideration, the effect of equivalence ratio on thermal performance is studied. Fig. 14 shows the temperature contours with overlaid 10% maximum HRR isoline for different equivalence ratio, which indicates that the combustor temperature level is decreasing and the flame front becomes obviously higher with the decrease of equivalence ratio. As a result, the temperature distribution is more uniform in the combustion chamber for a smaller equivalence ratio, as shown in Fig. 15. It displays the gas temperature profiles at the center axis of combustor for different equivalence ratio, which demonstrates that the maximum of gas temperature decreases from 1979.4 K at $\phi = 0.60$–1534.5 K at $\phi = 0.45$. These temperature distribution characteristics can significantly affect the thermal performances of solid walls, as discussed in the following section.

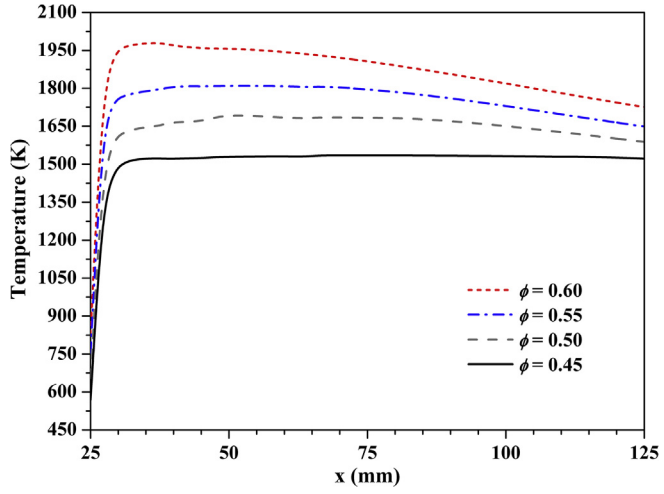

Fig. 15. Gas temperature profiles at the center axis of combustor ($z = 0.0$ mm, 25.0 mm $\leq x \leq$ 125.0 mm) for different equivalence ratio.

3.5.2. Effect of equivalence ratio on thermal performance

Here, the external surface of combustion chamber wall ($z = -10$ mm and 10 mm) serves as an example to discuss the effect of equivalence ratio on the thermal performance of each walls. Fig. 16a shows the temperature profiles of the inner surface at $z = -10$ mm for different equivalence ratio, which presents two peaks of temperature profile under a bigger equivalence ratio, but there is only one peak of temperature profile under a smaller equivalence ratio ($\phi = 0.45$). Furthermore, the wall temperature level is significantly decreasing with the decrease of equivalence ratio. The average center temperature of inner wall ($z = -10$ mm) at $\phi = 0.60$, $\phi = 0.55$, $\phi = 0.50$ and $\phi = 0.45$ are 802.4 K, 758.9 K, 705.3 K and 613.6 K, respectively. Specially, at $\phi = 0.45$, the wall temperature level in the downstream channel (~5.0 mm $\leq x \leq$ 80.0 mm) is obviously lower than that of other three equivalence ratios. In addition, the preheating area of inner wall is decreasing as the decrease of equivalence ratio, as shown in Fig. 17. It also presents that the surface area of heat loss obviously increases with a decreasing equivalence ratio, and the boundary between the preheating effect and heat loss effect areas becomes more disorder. This negative effect combining with the smaller heat release rate under a lower equivalence ratio leads to a lower gas temperature at the inlet of combustion chamber, as indicated in Fig. 16b. The calculated results indicate that the average gas temperature at the inlet of combustion chamber at y = 0.0 mm section for $\phi = 0.60$, $\phi = 0.55$, $\phi = 0.50$ and $\phi = 0.45$ are 698.2 K, 645.6 K, 578.9 K and 498.6 K, respectively.

4. Conclusions

A novel combustor combining the flow recirculation and heat recirculation effects is developed to further improve the flame stabilization. The experimental results show that the flame can remain symmetrically stable at very low equivalence ratio, which indicates that the present special structure has an excellent performance for anchoring the flame. Then, the thermal performance of each wall on the unburned mixture is studied. In the preheating channel at 5 mm $\leq z \leq$ 8 mm, the temperature of the unburned mixture near the flame holder is higher than that near the

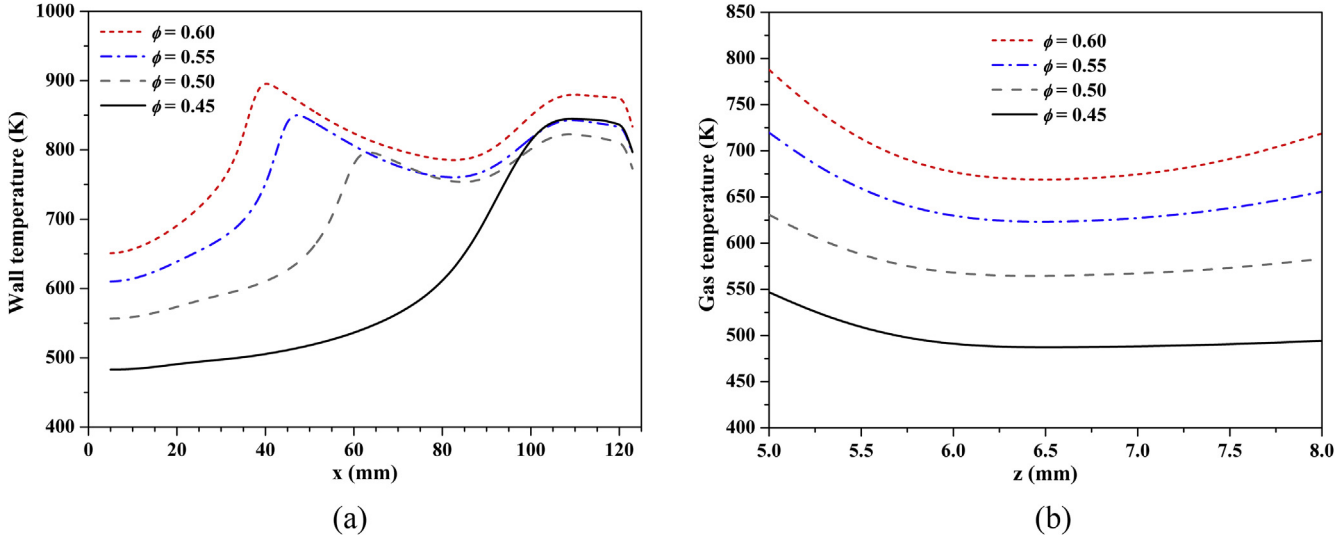

Fig. 16. Center temperature profiles of inner wall at $z = -10$ mm (5.0 mm $\leq x \leq$ 123.0 mm) (a) and the gas temperature profiles at the inlet of combustion chamber ($x = 25.0$ mm, 5.0 mm $\leq z \leq$ 8.0 mm) (b) at y = 0.0 section for different equivalence ratio.

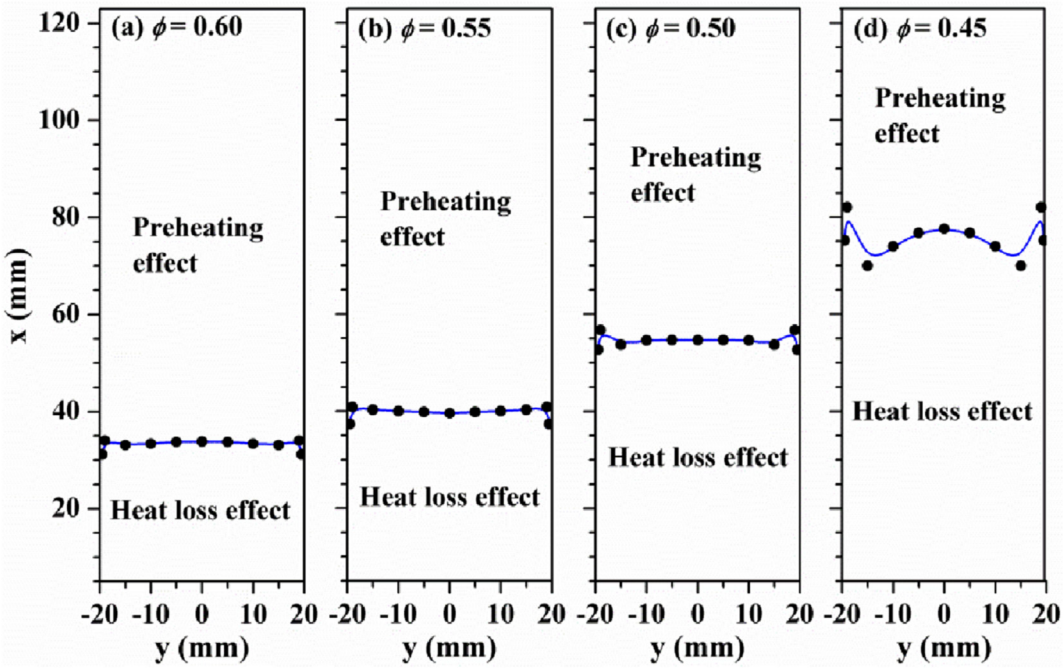

Fig. 17. The thermal performances of external surface of combustion chamber wall (z = −10 mm and 10 mm) on unburned mixture for different equivalence ratio.

combustion chamber wall, which indicates the unburned mixture is mainly preheated by the flame holder here. For the vertical wall of flame holder, the boundary of upper preheating area presents the "M" shape. However, the unburned mixture can be further preheated to a higher level in the combustion chamber by the inner surface of combustion chamber wall. In addition, the downstream part of combustion chamber wall absorbs heat from the burned mixture of high temperature. In the preheating channel at 10 mm $\leq z \leq$ 13 mm, the unburned mixture is mainly preheated by the external surface of combustion chamber wall due to the larger preheating area and higher wall temperature. The boundary between the preheating and heat loss areas of external surface of combustion chamber wall presents the "M" shape, but that of inner surface of preheating channel wall shows the upside-down pattern ("W" shape). These results indicate that the thermal performances of combustor wall on the unburned mixture are mainly determined by one side of higher temperature level (gaseous mixture side or solid wall side).

In addition, the flame height is obviously increasing with the decrease in the equivalence ratio. As a result, the distance between the two peaks of wall temperature profiles is shorter for a smaller equivalence ratio, and there is only one peak at $\phi = 0.45$. The preheating area decreases with a decreasing equivalence ratio, and the boundary between the preheating area and heat loss area becomes more disorder.

In summary, not every wall or the whole wall always has a preheating effect on the unburned mixture. Maybe some walls or some parts of walls play the negative effect of heat loss on the unburned mixture. A lower height of flame front results in a larger preheating area, which is probably beneficial for preheating the incoming unburned mixture. For instance, decreasing the width of flame holder or shortening the height of flame holder to a certain degree can improve the preheating effect. The present work can give guidance to optimize the present combustor with the special structure.

Acknowledgements

This work was supported by the Natural Science Foundation of China (Nos. 51706080, 51522603) and the China Postdoctoral Science Foundation (2016M600591).

Appendix A. Supplementary data

Supplementary data related to this article can be found at https://doi.org/10.1016/j.energy.2018.05.189.

References

[1] Ju Y, Maruta K. Microscale combustion: technology development and fundamental research. Prog Energy Combust Sci 2011;37(6):669–715.
[2] Shanbhogue SJ, Husain S, Lieuwen T. Lean blowoff of bluff body stabilized flames: scaling and dynamics. Prog Energy Combust Sci 2009;35(1):98–120.
[3] Maruta K, Kataoka T, Kim NI, Minaev S, Fursenko R. Characteristics of combustion in a narrow channel with a temperature gradient. Proc Combust Inst 2005;30(2):2429–36.
[4] Alipoor A, Mazaheri K. Studying the repetitive extinction-ignition dynamics for lean premixed hydrogen-air combustion in a heated microchannel. Energy 2014;73:367–79.
[5] Alipoor A, Mazaheri K. Combustion characteristics and flame bifurcation in repetitive extinction-ignition dynamics for premixed hydrogen-air combustion in a heated micro channel. Energy 2016;109:650–63.
[6] Pizza G, Frouzakis CE, Mantzaras J, Tomboulides AG, Boulouchos K. Dynamics of premixed hydrogen/air flames in microchannels. Combust Flame 2008;152(3):433–50.
[7] Brambilla A, Frouzakis CE, Mantzaras J, Bombach R, Boulouchos K. Flame dynamics in lean premixed/air combustion in a mesoscale channel. Combust Flame 2014;161(5):1268–81.
[8] Xu B, Ju Y. Experimental study of spinning combustion in a mesoscale divergent channel. Proc Combust Inst 2007;31(2):3285–92.
[9] Deshpande AA, Kumar S. On the formation of spinning flames and combustion completeness for premixed fuel–air mixtures in stepped tube microcombustors. Appl Therm Eng 2013;51(1–2):91–101.
[10] Kim N, Kato S, Kataoka T, Yokomori T, Maruyama S, Fujimori T, et al. Flame stabilization and emission of small Swiss-roll combustors as heaters. Combust Flame 2005;141(3):229–40.
[11] Kuo CH, Ronney PD. Numerical modeling of non-adiabatic heat-recirculating combustors. Proc Combust Inst 2007;31(2):3277–84.
[12] Chen W-H, Lin S-C. Reaction phenomena of catalytic partial oxidation of

methane under the impact of carbon dioxide addition and heat recirculation. Energy 2015;82:206–17.
[13] Jiang LQ, Zhao DQ, Guo CM, Wang XH. Experimental study of a plat-flame micro combustor burning DME for thermoelectric power generation. Energy Convers Manag 2011;52(1):596–602.
[14] Ning D, Liu Y, Xiang Y, Fan A. Experimental investigation on non-premixed methane/air combustion in Y-shaped meso-scale combustors with/without fibrous porous media. Energy Convers Manag 2017;138:22–9.
[15] Wang H, Wei C, Zhao P, Ye T. Experimental study on temperature variation in a porous inert media burner for premixed methane air combustion. Energy 2014;72:195–200.
[16] Veeraragavan A. On flame propagation in narrow channels with enhanced wall thermal conduction. Energy 2015;93:631–40.
[17] Kang X, Veeraragavan A. Experimental demonstration of a novel approach to increase power conversion potential of a hydrocarbon fuelled, portable, thermophotovoltaic system. Energy Convers Manag 2017;133:127–37.
[18] Wan JL, Fan AW, Maruta K, Yao H, Liu W. Experimental and numerical investigation on combustion characteristics of premixed hydrogen/air flame in a micro-combustor with a bluff body. Int J Hydrogen Energy 2012;37(24):19190–7.
[19] Wan JL, Fan AW, Yao H, Liu W. Experimental investigation and numerical analysis on the blow-off limits of premixed CH4/air flames in a mesoscale bluff-body combustor. Energy 2016;113:193–203.
[20] Wan JL, Fan AW, Yao H, Liu W. Effect of pressure on the blow-off limits of premixed CH4/air flames in a mesoscale cavity-combustor. Energy 2015;91:102–9.
[21] Yang WM, Chou SK, Shu C, Li ZW, Xue H. Combustion in micro-cylindrical combustors with and without a backward facing step. Appl Therm Eng 2002;22:1777–87.
[22] Zarvandi J, Tabejamaat S, Baigmohammadi M. Numerical study of the effects of heat transfer methods on CH4/(CH4 + H2)-AIR pre-mixed flames in a micro-stepped tube. Energy 2012;44(1):396–409.
[23] Zuo W, E J, Hu W, Jin Y, Han D. Numerical investigations on combustion characteristics of H 2/air premixed combustion in a micro elliptical tube combustor. Energy 2017;126:1–12.
[24] Zuo W, E J, Peng Q, Zhao X, Zhang Z. Numerical investigations on a comparison between counterflow and coflow double-channel micro combustors for micro-thermophotovoltaic system. Energy 2017;122:408–19.
[25] Yilmaz H, Cam O, Yilmaz I. Effect of micro combustor geometry on combustion and emission behavior of premixed hydrogen/air flames. Energy 2017;135:585–97.
[26] Baigmohammadi M, Tabejamaat S, Faghani-Lamraski M. Experimental study on the effects of mixture flow rate, equivalence ratio, oxygen enhancement, and geometrical parameters on propane-air premixed flame dynamics in non-adiabatic meso-scale reactors. Energy 2017;121:657–75.
[27] Yadav S, Yamasani P, Kumar S. Experimental studies on a micro power generator using thermo-electric modules mounted on a micro-combustor. Energy Convers Manag 2015;99:1–7.
[28] Fan AW, Zhang H, Wan JL. Numerical investigation on flame blow-off limit of a novel microscale Swiss-roll combustor with a bluff-body. Energy 2017;123:252–9.
[29] Wan JL, Fan AW. Effect of solid material on the blow-off limit of CH4/air flames in a micro combustor with a plate flame holder and preheating channels. Energy Convers Manag 2015;101:552–60.
[30] Wan JL, Fan AW, Yao H. Effect of the length of a plate flame holder on flame blowout limit in a micro-combustor with preheating channels. Combust Flame 2016;170:53–62.
[31] Xu Z, Zhao H. Simultaneous measurement of internal and external properties of nanoparticles in flame based on thermophoresis. Combust Flame 2015;162(5):2200–13.
[32] Xu Z, Tian X, Zhao H. Tailor-making thermocouple junction for flame temperature measurement via dynamic transient method. Proc Combust Inst 2017;36(3):4443–51.
[33] Fluent 14.0. User's guide. 2011. Canonsburg, PA.
[34] Kee RJ, Grcar JF, Smooke MD, Miller JA. Sandia national laboratories report, SAND85–8240. 1994.
[35] Kee RJ, Rupley FM, Miller JA. Sandia national laboratories report, SAND87–8215B. 1990.
[36] Kee RJ, Grear JF, Smooke MD, Miller JA. Sandia national laboratories report, SAND85–8240. 1985.
[37] Holman JP. Heat transfer. 9th ed. New York: McGraw-Hill; 2002.
[38] Ma Q, Fang R, Xiang L. Handbook of thermo-physical properties. Beijing: China Agricultural Machinery Press (in chinese); 1986.
[39] Lee BJ, Yoo CS, Im HG. Dynamics of bluff-body-stabilized premixed hydrogen/air flames in a narrow channel. Combust Flame 2015;162(6):2602–9.